Journal of Theoretical Biology 353 (2014) 121–132

Contents lists available at ScienceDirect

Journal of Theoretical Biology

journal homepage: www.elsevier.com/locate/yjtbi

Exploiting elasticity: Modeling the influence of neural control on mechanics and energetics of ankle muscle–tendons during human hopping

Benjamin D. Robertson [a,b], Gregory S. Sawicki [a,b]

[a] Joint Department of Biomedical Engineering, University of North Carolina, Chapel Hill, NC, United States
[b] North Carolina State University, Raleigh, NC, United States

HIGHLIGHTS

- We present a simplified model of human ankle driven hopping.
- We examine how simple neural control governs system dynamics.
- Hopping safely achieved at human-like frequencies (i.e. 2.2–3.4 Hz).
- Peak mechanical "tuning" observed at frequencies above passive resonance.
- Stimulation amplitude governs metabolic rate, peak active force in muscle.

ARTICLE INFO

Article history:
Received 18 August 2013
Received in revised form
13 January 2014
Accepted 7 March 2014
Available online 16 March 2014

Keywords:
Plantarflexors
Locomotion
Muscle mechanics
Metabolic cost
Elastic mechanisms

ABSTRACT

We present a simplified Hill-type model of the human triceps surae-Achilles tendon complex working on a gravitational–inertial load during cyclic contractions (i.e. vertical hopping). Our goal was to determine the role that neural control plays in governing muscle, or contractile element (CE), and tendon, or series elastic element (SEE), mechanics and energetics within a compliant muscle–tendon unit (MTU). We constructed a 2D parameter space consisting of many combinations of stimulation frequency and magnitude (i.e. neural control strategies). We compared the performance of each control strategy by evaluating peak force and average positive mechanical power output for the system (MTU) and its respective components (CE, SEE), force–length (F–L) and –velocity (F–V) operating point of the CE during active force production, average metabolic rate for the CE, and both MTU and CE apparent efficiency. Our results suggest that frequency of stimulation plays a primary role in governing whole-MTU mechanics. These include the phasing of both activation and peak force relative to minimum MTU length, average positive power, and apparent efficiency. Stimulation amplitude was primarily responsible for governing average metabolic rate and *within* MTU mechanics, including peak force generation and elastic energy storage and return in the SEE. Frequency and amplitude of stimulation both played integral roles in determining CE F–L operating point, with both higher frequency and amplitude generally corresponding to lower CE strains, reduced injury risk, and elimination of the need for passive force generation in the CE parallel elastic element (PEE).

1. Introduction

Decades of research on the mechanics and energetics of locomotion has established the role of passive elastic tissues (e.g. tendons, aponeuroses) in shaping efficient and stable movement (Geyer et al., 2006; Alexander, 2002; Hof et al., 2002; Ishikawa et al., 2005; Lichtwark et al., 2007; Lichtwark and Wilson, 2008; Lichtwark and Wilson, 2007; van der Krogt et al., 2009; Takeshita et al., 2006). This concept is best illustrated by simple spring-based models of human locomotion that predict walking (Geyer et al., 2006; Holt et al., 1990; Srinivasan and Holmes, 2008), running (Geyer et al., 2006; Srinivasan and Holmes, 2008; Blickhan, 1989), and hopping (Blickhan, 1989; Farley and Morgenroth, 1999) mechanics in the absence of any active components (i.e. muscles). These purely elastic models successfully predict center of mass mechanics and are intrinsically stable, but they ignore the contribution of active muscle resonant behavior in the coupled muscle–tendon system.

Other simple modeling frameworks have explored the role that *only* active tissues play in cyclic force/power production and stability of movement (Haeufle et al., 2010, 2012). Purely muscle-based models can address questions related to the extent that

http://dx.doi.org/10.1016/j.jtbi.2014.03.010
0022-5193/

feed-forward and feedback based neuromuscular control in conjunction with non-linear force–length and –velocity dynamics can stabilize perturbed movements (Haeufle et al., 2010, 2012). However, these models lack key elastic tissues; both series tendon/aponeurosis *and* parallel structures that can generate force passively in muscle. Both series and parallel elastic tissues can alter the force and length trajectories of the muscle contractile elements, but few models take into account combined muscle–tendon architecture. Models that include series elasticity have given important insight into the role of elastic tissues in optimizing movement (i.e. walking running, jumping, swimming) for minimum metabolic cost, maximum efficiency or maximum mechanical power output (Alexander, 1997; Roberts, 2002; Srinivasan, 2011). None of these studies, however, directly explores how neural control pattern modulates muscle–tendon interaction dynamics during cyclic contractions.

More complex modeling frameworks have been developed for examining the interplay of many muscle–tendon units of the lower limbs during walking, running, and hopping. These models incorporate complex limb geometries with distributed mass, physiologically accurate muscle and tendon architecture, and can track joint-level kinematics and kinetics to predict neuromuscular control patterns with similar timing and magnitude to those observed experimentally (Krishnaswamy et al., 2011; Arnold and Delp, 2011; Bobbert et al., 1986; Neptune and McGowan, 2011; Neptune et al., 2009; Umberger and Rubenson, 2011; Arnold et al., 2013). This is extremely useful for examining the role of elastic tissues in shaping whole limb, joint, and muscle-level mechanics and energetics (Neptune et al., 2009; Umberger and Rubenson, 2011; Umberger et al., 2003). Complex musculoskeletal models have also been used to predict locomotion behavior based on optimization of some objective function ((i.e. minimal metabolic cost/muscle activation and maximum height jumping) (Ackermann and van den Bogert, 2010). However, it is unclear that there is a single underlying factor that humans seek to optimize as part of functional gait (Carrier et al., 2011; Monsch et al., 2012), motivating the need for studies that examine performance along multiple objectives (i.e. metabolic cost, injury risk, stability, and efficiency)

Our goal in this study was to develop a simple framework to examine the fundamental aspects of how neural control (e.g. frequency and magnitude of stimulation) mediate muscle–tendon unit (MTU) dynamics during functional movement. For example, utilizing active muscle versus passive elastic tissues to modulate compliant limb/joint mechanics may allow for more robust control, but also requires consumption of additional metabolic energy – an important trade-off that may shape preferred movement strategies. Many studies have shown that a coupled muscle–tendon system can significantly reduce energy costs with little effect on overall power output by minimizing muscular length change, and maximizing energy storage and return in series elastic tissues (Geyer et al., 2006; Hof et al., 2002; Takeshita et al., 2006; Snyder and Farley, 2011; Dean and Kuo, 2011; Raburn et al., 2011). Under these conditions, the muscle is said to be contracting isometrically, and the muscle–tendon unit (MTU) is "tuned" to exploit compliance. When a MTU becomes tuned there are significant reductions in contractile element (CE) mechanical power and increases in peak force; both of which likely play an important role in overall metabolic cost and efficiency of movement (Takeshita et al., 2006; Krishnaswamy et al., 2011; Dean and Kuo, 2011; Raburn et al., 2011). The benefits of an optimally tuned MTU are clear, but the role of the central nervous system in coordinating the timing and magnitude of muscle activation to optimize elastic energy storage in and return in series elastic elements (SEE) is not.

In this study we explored how a compliant MTU responded to different frequencies and magnitudes of stimulation during a simple, rhythmic movement (i.e. human hopping) that relies heavily (up to ~80% of limb total positive mechanical power) on the ankle muscle–tendon units (i.e. triceps-surae Achilles tendon complex) to perform the mechanical work required by the task (Farris and Sawicki, 2012). To simplify the model, we lumped the triceps-surae muscle group into a single, monoarticular muscle with a series tendon and a fixed mechanical advantage (Fig. 1). We started our exploration of possible operating frequencies by first finding the resonant frequency ($\omega_{MTU\ resonance}$) of the passive mechanical system under the load of the body in the absence of any CE activation. For the system detailed here, we found $\omega_{MTU\ resonance}$ = 2.1 Hz. We hypothesized that stimulating this compliant muscle–tendon system at $\omega_{MTU\ resonance}$ would "tune" the mechanical system and (1) maximize MTU force generation and elastic energy storage and return in the SEE and (2) minimize CE work for any given stimulation amplitude. We also expected that (3) the amplitude of muscle stimulation would modulate force/power production between CE and SEE within the MTU. Finally, we predicted that, owing to the fact that low velocity contractions are metabolically inexpensive (Minetti and Alexander, 1997), driving the MTU at $\omega_{MTU\ resonance}$ would (4) minimize metabolic rate and maximize MTU apparent efficiency.

2. Methods

To investigate the effect that neural control has on the mechanics and energetics of human hopping we developed a mathematical model of a cyclically stimulated compliant MTU (i.e. bouncing gait). The model included a massless Hill-type muscle and parallel elastic element (PEE) collectively referred to here as the CE, in series with a non-linear tendon-spring, or SEE, operating with a fixed mechanical advantage on a point mass experiencing constant gravitational forces; which captures the muscle–tendon dynamics at distal joints of the lower-limb (e.g. ankle) (Fig. 1). To approximate mechanical properties of the human triceps-surae Achilles tendon complex, several key simplifications were made. First and foremost, we combined the gastrocnemii and soleus muscles into a single, monoarticular, muscle. This disregards the fact that the gatrocnemii muscles act across both the ankle and knee joints, which will limit our models ability to reliably predict MTU mechanics under conditions where humans no longer exhibit spring-like behavior and employ deep knee bends as part of

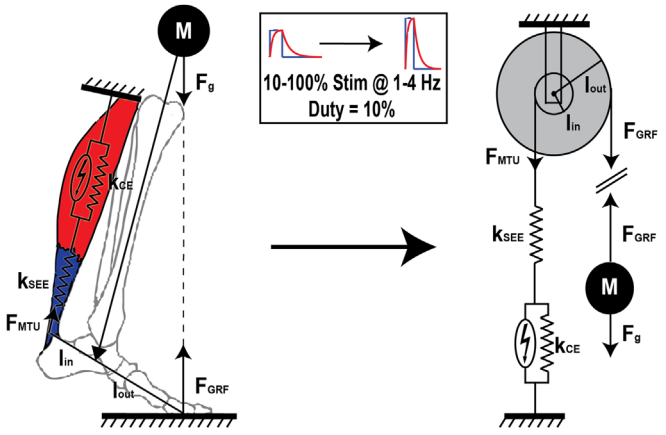

Fig. 1. Physiological basis for (left), and mechanical schematic of (right), lumped triceps surae-Achilles tendon group interacting with mass in gravity. Parameter space traversed is indicated in the box between the two schematics. Control parameters acted upon active elements of modeled system, indicated by encircled lighning bolts. System parameters and equations can be seen in Tables 1 and 2, respectively.

functional gait (i.e. low frequency hopping, $\leq \sim 2.0$ Hz) (Farley et al., 1991). Secondly, we model our lumped triceps-surae muscle group as non-pennate. Experimental studies exploring decoupling of fascicle and whole-muscle length/velocity dynamics due to pennation have demonstrated that there is little difference between the two under high force conditions like those modeled here (Azizi et al., 2008). Third, the mechanical advantage of this system was fixed, disregarding shifts in moment arm length that occur in an intact biological system during overground gait (i.e. walking and running) (Carrier et al., 1994; Biewener et al., 2004). We believe this to be a reasonable approximation for hopping, as there are no dramatic shifts in center of pressure over the course of ground contact as might be observed in forward progression (Carrier et al., 1994; Biewener et al., 2004; Maykranz et al., 2013). Fourth, there are no antagonist muscles in this model; cyclic mechanics arose from interplay between our modeled triceps surae and gravitational and inertial forces acting on a point mass. Our mass was modeled as half body mass to approximate loads experienced during two-legged hopping. Finally, there were no set configuration for a flight phase. There was, however, an "aerial" portion in which MTU–load coupling goes slack for a large portion of modeled conditions, and the only force remaining is gravitational (Figs. 2 and 3A). Model parameters and equations can be found in Tables 1 and 2, respectively.

2.1. Muscle activation dynamics

Force is generated in our modeled CE by a Hill-type muscle with classic, normalized, non-linear force–length (F–L) and –velocity (F–V) relationships, and non-linear PEE with slack length l_0 based on equations from Azizi et al. (Azizi and Roberts, 2010; Otten, 1987; Fung, 1967) (Table 2). Experimental measurements used to derive human F–L fit values were generously provided by Rubenson et al. (2012). Normalized F–V curves were taken from Haeufle et al. (2010) and based on experimental curves from Hill (1938).

Stimulation was modeled as a square wave pulse that had a duty equal to 10% of the cycle period T_{stim} (i.e. $T_{stim} = \omega_{stim}^{-1}$, stimulation duty$= 0.1 \times T_{stim}$) (Fig. 2). This square wave was subject to a first order excitation-activation coupling dynamics to generate a corresponding activation function $\alpha(t)$ to drive muscular contraction, resulting in an activation/active force duration of 50–80% of a cycle. These values are in agreement with experimentally observed force/EMG duties (Farris and Sawicki, 2012; Farris et al., 2013, 2006; Zajac, 1989) (Fig. 2). Force generated by the CE was equal to

$$F_{CE} = F_{max} \times \alpha(u(t), \tau_{act}, \tau_{deact}) \times F_{l\ active}(l_{CE}, l_0) \times F_v(v_{CE}, v_{max}) + F_{l\ passive}(l_{CE}, l_0)$$

where F_{CE} is total CE force, F_{max} was maximum active isometric force possible from the CE, $\alpha(u(t), \tau_{act}, \tau_{deact})$ was normalized muscle activation in terms of periodic square-wave stimulation $u(t)$, as well as muscle activation (τ_{act}) and relaxation (τ_{deact}) time constants (Krishnaswamy et al., 2011; Zajac, 1989). Time constants were determined by taking a weighted average of reported values for medial/lateral gastrocnemius and soleus based on their peak cross-sectional area (Winters and Stark, 1988; Raasch et al., 1997; Fukunaga et al., 1992). F_l was instantaneous normalized F–L operating point as a function of muscle length (l_{CE}) and l_0 for muscle. F_v was instantaneous normalized F–V operating point in terms of rate of muscular length change (v_{CE}) and v_{max} for the CE. Normalized F–L and F–V relationships are visualized in Fig. 7, and their equations can be seen in Table 2. Muscle and system parameter values used were based on literature values for human plantarflexors and can be found in Table 1.

2.2. Tendon dynamics

The SEE in our compliant MTU was modeled with a non-linear "toe" region at operating points just above the slack length, after which its stiffness can be approximated as linear (Lichtwark et al., 2007; Lichtwark and Wilson, 2008, 2007). Forces generated in the SEE are described by the following relationship:

$$F_{SEE} = \begin{cases} 0 & l_{SEE} \leq l_{slack} \\ k_{SEE}(k_t, F_{CE}) \times (l_{SEE} - l_{slack}) & l_{SEE} > l_{slack} \end{cases}$$

where k_{SEE} was the stiffness function for the tendon (Table 2), l_{SEE} was the length of the SEE, and l_{slack} was the slack length of the SEE, below which it cannot store or return energy.

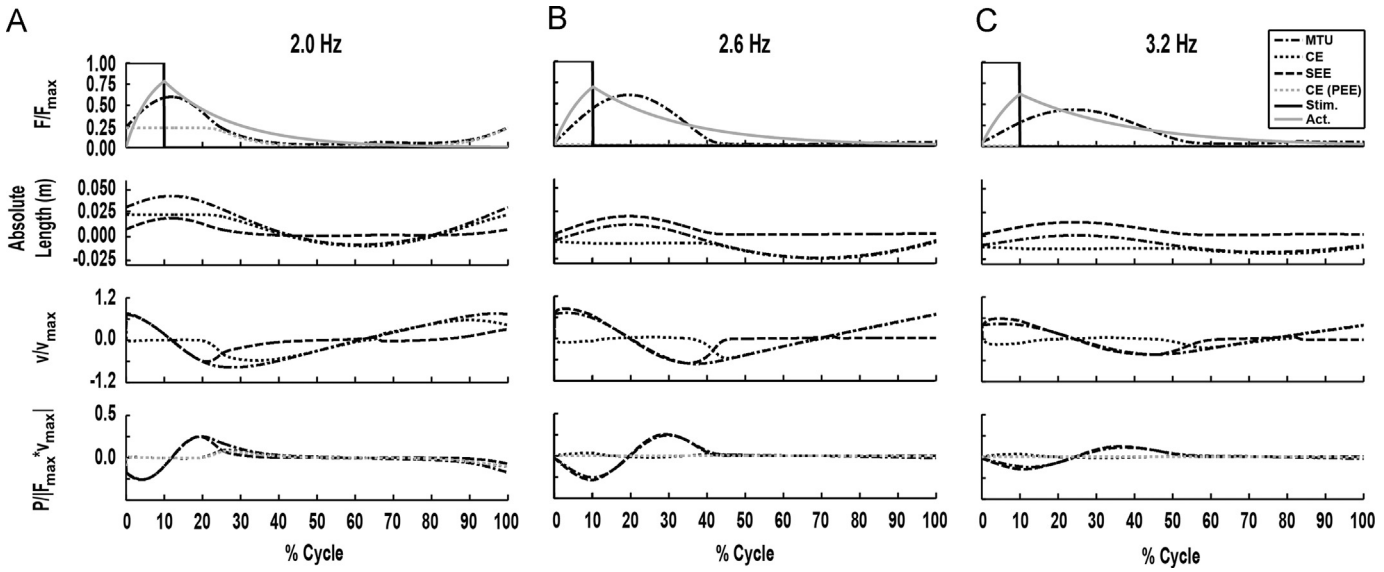

Fig. 2. Periodic data for 100% stimulation amplitude condition at frequencies of (A) 2.0 Hz, (B) 2.6 Hz, and (C) 3.2 Hz. Each data set contains normalized stimulation/activation and force dynamics (top, F/F_{max}), absolute length (first from top, $l_{CE}^{abs} = l_{CE} - l_0$, $l_{SEE}^{abs} = l_{SEE} - l_{slack}$, $l_{MTU}^{abs} = l_{MTU} - (l_0 + l_{slack})$), normalized velocity (second from top, v/v_{max}), and normalized power (bottom, $P/|F_{max} \times v_{max}|$) (Table 1). Each data set is plotted for a single period of stimulation relative to stimulation onset (0% of cycle). Note well defined regions of high force production ("ground contact"), and regions where $F/F_{max} = 0$ ("flight") at every stimulation frequency.

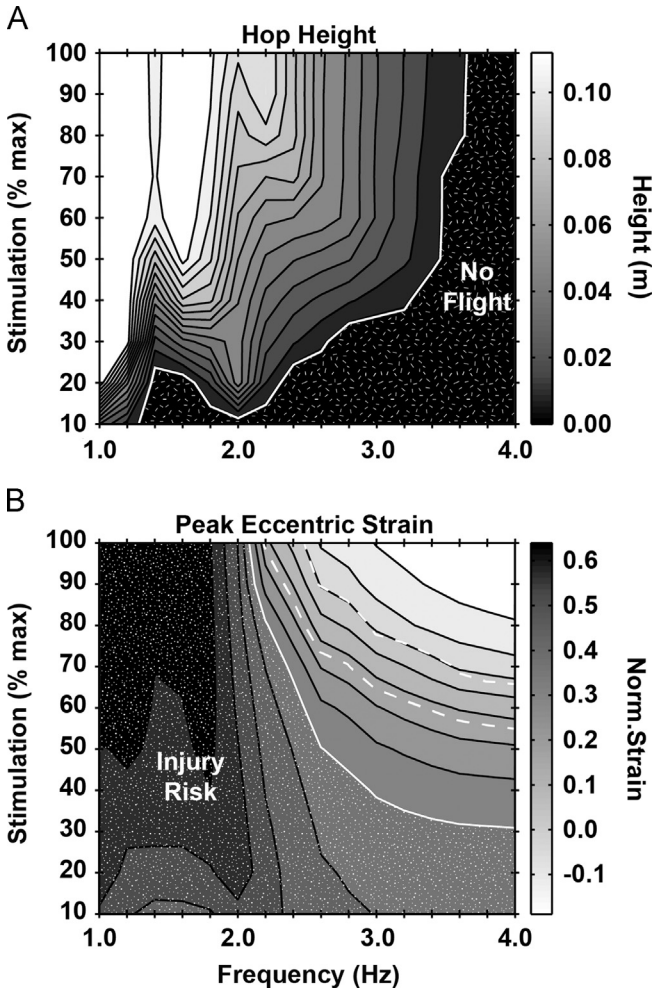

Fig. 3. (A) Hop height (contours) versus frequency (x-axis) and amplitude (y-axis) of stimulation. Conditions which did not achieve flight are indicated by a white border and hatched region labeled "no flight". These primarily include high stimulation frequency and low stimulation amplitude regions of parameter space. (B) Normalized peak eccentric CE strain (contours) versus stimulation frequency (x-axis) and amplitude (y-axis). Regions of high injury risk are indicated by a white border and speckled region labeled "injury risk", and generally occur at frequencies ≤ 2.0 Hz. The region outlined by the white dashed line indicates an average operating strain of $\pm 1.05 l_0$ during active force production.

Table 1
Parameter values used in model implementation.

	Value
Muscle parameters (CE)	
F_{max}	6000 N (Hof et al., 2002; Lichtwark and Wilson, 2007; Krishnaswamy et al., 2011)
v_{max}	−0.45 m/s (Hof et al., 2002; Lichtwark and Wilson, 2007)
l_0	0.055 m (Lichtwark and Wilson, 2007, 2008)
k_m	90,000 N/m (Lichtwark and Wilson, 2008, 2007)
Tendon parameters (SEE)	
l_{slack}	0.237 m (Lichtwark and Wilson, 2008, 2007)
k_t	180,000 N/m (Lichtwark and Wilson 2008, 2007)
Activation parameters	
τ_{act}	0.033 s (Winters and Stark, 1988; Raasch et al., 1997)
τ_{deact}	0.091 s (Winters and Stark, 1988; Raasch et al., 1997)
Pulse duty	10.0%
Environment dynamics	
g	9.8 m/s^2
EMA(l_{in}/l_{out})	0.33 (Lichtwark and Wilson, 2007)
M	35 kg[a]

[a] Half body mass.

2.3. Model implementation

Periodic excitation of the "lumped" triceps-surae Achilles tendon MTU was modeled for a range of stimulation values (10–100% of maximum) and frequencies (1–4 Hz) about the resonant frequency of the passive mechanical system ($\omega_{MTU\ resonance} \sim 2.1$ Hz). All simulations were run for 15 s with a fixed time step ($dt = 0.0005$ s) and used the 4th order Runge–Kutta method to solve for system dynamics (MATLAB 2010b, MathWorks Inc). The last four cycles of stimulation were used in final analysis to be sure that the system had ample time to settle into steady-state mechanics.

2.4. Performance metrics

2.4.1. Periodic behavior

The relationship between ω_{MTU}, the frequency of MTU mechanical output, and ω_{stim}, the frequency of stimulation input, was of fundamental interest in this study. There was an assumed relationship:

$$\omega_{MTU} = n \times \omega_{stim}$$

where n is a scalar multiple. To determine periodicity with stimulation, we developed a metric dubbed the "integrated return map" (IRM) based on the variability of MTU length (l_{MTU}) and velocity (v_{MTU}) dynamics within each of the K cycles included in final analysis (for all work presented here, $K=4$). First we averaged $l_{MTU}(t)$ and $v_{MTU}(t)$ values from each of our K cycles for every timepoint $t = [0, T_{stim}]$ within a given cycle of stimulation, with T_{stim} being the period of stimulation (i.e. $T_{stim} = \omega_{stim}^{-1}$). Mean position ($\bar{l}_{MTU}(t)$) and velocity ($\bar{v}_{MTU}(t)$) values were computed as follows:

$$\bar{l}_{MTU}(t) = \left(\sum_{k=1}^{K} l_{MTU}(t,k) \right) / K, \quad \bar{v}_{MTU}(t) = \left(\sum_{k=1}^{K} v_{MTU}(t,k) \right) / K$$

The absolute difference between average and individual $l_{MTU}(t)$ and $v_{MTU}(t)$ values was then integrated over period T_{stim} for K cycles used in analysis, and summed to determine an IRM value for each condition as follows:

$$\mathrm{IRM}(\omega_{stim}, A_{\mathrm{stim}}) = \sum_{k=1}^{K} \left[\int_{t=0}^{T_{stim}} [|l_{MTU}(t,k) - \bar{l}_{MTU}(t)| + |v_{MTU}(t,k) - \bar{v}_{MTU}(t)|] \times dt \right]$$

where ω_{stim} and A_{stim} were the frequency and magnitude of stimulation for each experimental condition. IRM values within an acceptable range to be considered round off error (i.e. IRM ≈ 0), indicate dynamics that were cyclic with stimulation, or had period one dynamics (i.e. $\omega_{MTU} = \omega_{stim},\ n = 1$). Conditions exhibiting $n \neq 1$ mechanics (i.e. $\omega_{MTU} \neq \omega_{stim}$) had IRM values several orders of magnitude larger than those for $n=1$ conditions (i.e. IRM $\neq 0$).

2.4.2. Flight phase

Hopping was considered to encompass any emergent behavior consisting of alternating flight and ground contact phases. Flight was defined as any instance where our point mass acceleration was equal to that of gravity (e.g. $F_{net} = Mg$, Table 1).

2.4.3. Injury risk and average strain

Injury risk was determined based on peak eccentric engineering strain using the following equation:

$$\epsilon_{peak} = \max\left((l_{CE}(t) - l_0)/l_0\right) \quad \text{when } (dl_{CE}(t)/dt) > 0$$

High potential for injury was associated with $\epsilon_{peak} > 0.3$ based on in vitro experiments in animal tissues (Lieber and Friden, 1993; Lieber et al., 1991a,b; Brooks et al., 1995; Morgan and Allen, 1999).

We also chose to examine the average CE strain during active force production to evaluate what, if any, conditions operated closest to l_0 while the muscle was in an active state. Average strain

Table 2
Equations and parameter values used in model implementation.

	Equation	Values
Muscle force–length		
F_l active	$e^{-\lvert((l_m/l_0)^b - 1)/s\rvert^a}$ (Azizi and Roberts, 2010; Otten, 1987)	$b=0.8698$, $s=0.3914$, $a=3.1108$
F_l passive	$A \times e^{(b*((l_m/l_0)-1))}$ (Azizi and Roberts, 2010; Otten, 1987)	$A=2.38\times10^{-2}$, $b=5.31$
Muscle force–velocity		
F_v when $v_m>0$	$(1-(v_{CE}/v_{max}))/(1+(v_{CE}/(k\times v_{max})))$ (Haeufle et al., 2010; Hill, 1938)	$k=0.17$
F_v when $v_m<0$	$1.8-0.8\times((1+v_{CE}/v_{max})/(1-7.56\times(v_{CE}/(k\times v_{max}))))$ (Haeufle et al., 2010; Hill, 1938)	$k=0.17$
Tendon stiffness		
k_{SEE}	$k_t\times(1+(0.9/-e^{((Q\times F_{CE})/F_{max})}))$ (Lichtwark and Wilson, 2008)	$Q=20$
Activation dynamics		
$\alpha(t)$	$\int[(u(t)/\tau_{act})-(1/\tau_{act})\times(\beta+(1-\beta)\times u(t))]\,dt$ Zajac, 1989	$\beta=\tau_{act}/\tau_{deact}$
Metabolic rate		
$p(v_{CE})$ for $v_{CE}>1$	$0.01-0.11\,(v_{CE}/v_{max})+0.06e^{(-8v_{CE}/v_{max})}$ Alexander, 1997	–
$p(v_{CE})$ for $v_{CE}>1$	$0.23-0.16e^{(-8v_{CE}/v_{max})}$ (Alexander, 1997)	–

was evaluated as follows:

$$\bar{e}_{CE} = \text{mean}(\text{abs}((l_{CE}(t)-l_0)/l_0)) \quad \text{when} \quad \alpha(u(t),\tau_{act},\tau_{deact})>0.01$$

2.4.4. Peak force

To further assess mechanical performance we computed peak MTU force over a cycle of stimulation. MTU peak force is equivalent to peak forces produced in both the CE and SEE, and is a good indicator of the amount of elastic energy cycling in the SEE.

The peak value of force was taken for each of the four cycles used in analysis, normalized to F_{max}, and averaged for all conditions. The CE can produce force both actively *and* passively at operating lengths greater than l_0. To understand how active and passive elements of CE contribute to total CE force we computed the percentage from each as follows:

$$\%F^{max}_{CE\ active} = F_{CE\ active}(t_{max})/F_{MTU}(t_{max})\times 100$$

where $F_{CE\ active}$ is force produced actively in the CE, and t_{max} is the time of peak MTU force for a given cycle. The percentage of contribution to F^{max}_{MTU} from passive elements in the CE adhered to the relationship:

$$\%F^{max}_{CE\ passive} = 100-\%F^{max}_{CE\ active}$$

2.4.5. Stimulation and peak force phase metrics

To assess the whether or not stimulation onset timing was a contributing factor in hopping behavior, we assessed the average phasing of the time of both CE stimulation onset and MTU peak force in a cycle of hopping relative to the time within a given cycle when MTU is at its shortest length. These phase delays are reported as a percentage of the period of stimulation, $T_{stim}=\omega^{-1}_{stim}$.

2.4.6. Average positive mechanical power

To asses mechanical output of the MTU and its components we computed average positive power (i.e. rate of mechanical work) produced over a cycle of stimulation. We chose average power because mechanical work performed on the load (i.e. COM) has been strongly associated with metabolic cost of movement (Dean and Kuo, 2011; Doke and Kuo, 2007; Kuo et al., 2005). We used average *positive* power because SEE's can only cycle energy, and their net power production over a cycle of stimulation is zero for period one mechanics. For a given stimulation frequency ω_{stim}, and ignoring power outputs less than zero:

$$\bar{P}^{+}_{mech} = \left[\int_{t=0}^{T_{stim}} P^{+}_{mech}(t)\,dt\right]\times\omega_{stim}$$

where $\bar{P}^{+}_{mech}$ is average positive mechanical power produced over a cycle of stimulation, $P^{+}_{mech}(t)$ is positive mechanical power as a function of time, and T_{stim} is the period of stimulation. All stimulation cycles used for analysis were averaged to ensure a reasonable representation for conditions where $n\neq 1$. This method was used to compute average power from the MTU, CE, and SEE with all values normalized to $|F_{max}\times v_{max}|$ for the CE (Table 1).

While overall MTU mechanics are of great importance, our model allowed us to decouple these mechanics to explore CE and SEE contributions. To this end, we looked at the percentage of total positive power produced over a cycle by the CE as follows:

$$\%\bar{P}^{+}_{mech\ CE} = (\bar{P}^{+}_{mech\ CE}/(\bar{P}^{+}_{mech\ CE}+\bar{P}^{+}_{mech\ SEE}))\times 100$$

where $\%\bar{P}^{+}_{CE}$ is the average percentage of total positive power over a cycle of stimulation from the CE, and $\bar{P}^{+}_{CE}$ and $\bar{P}^{+}_{SEE}$ are positive power as a function of time for the CE and SEE, respectively. The percent contribution from SEE was assumed to adhere to the relationship:

$$\%\bar{P}^{+}_{SEE} = 100-\%\bar{P}^{+}_{CE}$$

Standard deviations for $\%\bar{P}^{+}$ were also computed to observe variations from average values for the $n\neq 1$ case.

2.4.7. Metabolic power and apparent efficiency

To assess metabolic performance of different control strategies we calculated average metabolic rate, and associated apparent MTU and CE efficiencies. Metabolic rate was determined based on CE velocity, and scaled by activation, using a model taken from (Krishnaswamy et al., 2011)

$$P_{met}(t) = p(v_{CE}(t))\times\alpha(t)\times|F_{max}\times v_{max}|$$

where $P_{met}(t)$ is instantaneous metabolic rate at time t, and $p(v_{CE}(t))$ is a cost function taken from (Alexander, 1997; Ma and Zahalak, 1991) and shown in Table 2. Average metabolic rate for each condition was computed by integrating instantaneous metabolic cost for each period, multiplying by frequency (i.e. dividing by period), and dividing by the system mass M (Table 1) to get units of units of W/kg:

$$\dot{\bar{P}}_{met} = \left[\int_{0}^{T_{stim}} P_{met}(t)\,dt\right]\times(\omega_{stim}/M)$$

Apparent efficiency of positive mechanical work was also determined for each experimental condition to examine how different neural control strategies utilize metabolic energy to perform mechanical work on the load. Apparent efficiency of positive mechanical

work for each component (e.g. MTU, CE) was determined as follows:

$$\bar{e}_{met} = \left(\int_0^{T_{stim}} P^{+}_{mech}(t)\,dt\right) / \left(\int_0^{T_{stim}} P_{met}(t)\,dt\right)$$

where $\bar{e}_{met}$ is average apparent efficiency, P^{+}_{mech} is positive mechanical work, and P_{met} is metabolic cost. Apparent efficiency can be related to the fraction of average positive mechanical power contributed by the CE versus the SEE (i.e. muscle work fraction$=0.25/\bar{e}_{met}$) (Sawicki and Ferris, 2008).

3. Results

3.1. Periodic mechanics

Most stimulation frequency–amplitude combinations resulted in behavior that was periodic with stimulation onset (i.e. $n=1$) (Fig. 2). The only notable exception to this was for low frequency stimulations ($\omega_{stim} < 1.4$), for which mechanical behavior was period two ($n=2$) and each cycle of stimulation resulted in two hops; one driven by active muscle, and one driven by purely passive forces in the MTU.

3.2. Flight phase

A flight phase was observed for all stimulation frequencies less than ~3.4 Hz. Flight required the least stimulation amplitude for frequencies in the 2.0–2.2 Hz range (Fig. 3A). Conditions that did not achieve flight are indicated by a speckled region bordered in white and labeled "no flight" in all relevant figures.

3.3. Peak and mean CE strain

Peak strains associated with elevated risk of injury ($\epsilon_{peak} > 0.3$) occurred at every frequency for stimulation amplitude below 30% of maximum (Fig. 3B). In general, lower stimulation frequencies required higher stimulation amplitude to keep peak strain below 0.3. For stimulation frequencies >2.0 Hz, risk of injury could be drastically reduced by increasing stimulation amplitude by amounts that vary depending on the frequency of operation (Fig. 3B). While it is entirely possible for humans to hop outside the range of frequencies constrained by this criteria, deep knee bends would be required to reduce injury risk. As a result, these conditions would no longer be considered "ankle driven", and predictions made by this model are unlikely to be reflective of human behavior.

Values of average CE strain during active force production also showed both strong stimulation frequency and amplitude dependence. For frequencies ≥ 2.2 Hz, it is possible to remain at an average operating length $\sim l_0$ (i.e. $\pm 0.05 l_0$, ± 2.75 mm) with the proper stimulation amplitude. This region of parameter space is bordered in white dashed lines in (Fig. 3A and B) and all subsequent contour plots. From the region bordered in white, if stimulation magnitude or frequency is increased, the average CE operating length will fall below l_0 onto the ascending limb of F–L (Fig. 7A and C); but if stimulation magnitude or frequency is decreased, the average CE operating length will rise above l_0 onto the descending limb of F–L. It is worth noting that, while a mean operating strain of $\pm 0.05 l_0$ allows for a peak isometric force of F_{max}, mean operating strains of $\pm .2 l_0$ (± 11 mm) can still produce active forces $\geq 0.9 F_{max}$. This leads to a broad range of operating points capable of producing high active forces without excessive risk of injury.

3.4. Peak force

Peak MTU (as well as CE and SEE) forces were observed in the 2.2–2.4 Hz range and maximal (100%) stimulations (Fig. 4). At frequencies ≤ 1.8 Hz, peak forces were almost entirely the result of passive forces in the CE. As frequency of stimulation increased, so too did active contributions to CE force (Fig. 5). The extent to which active forces contribute to CE force production was also dependent on stimulation amplitude. At 70% of maximum stimulation all frequencies required at least some contribution from the CE PEE (e.g. at 2.4 Hz, ~15% of total force is from the PEE) (Fig. 5D). For maximal stimulation (100%), all CE force was produced actively for stimulation frequencies ≥ 2.6 Hz (Fig. 5B). Conditions in which passive CE force played a significant role also posed significant risk of injury (Figs. 3B and 5A and C).

3.5. Stimulation and peak force phasing

Phasing of stimulation onset relative to MTU minimal length underwent a relatively sharp transition, dropping from ~70% to ~30% near the passive resonant frequency (~2.1 Hz) (Figs. 2 and 6A). Furthermore, for combinations of frequency and magnitude of stimulation between 1.6 and 3.6 Hz and stimulation amplitudes $\geq 50\%$, there is a well-defined "ground contact" phase that is nearly coincident with stimulation onset, resulting in peak forces that occur consistently at 50% of a cycle following the time of MTU shortest length (Fig. 6B). For frequencies <1.8 Hz there were two cycles of ground contact and flight per period of stimulation, one driven entirely by passive mechanics and the other by muscle activation. This ultimately resulted in peak force preceding stimulation onset for these conditions (Fig. 6). Phasing of stimulation onset and peak MTU force did not depend strongly on stimulation amplitude (Fig. 6).

3.6. CE operating length and velocity

CE operating length and velocity had both stimulation frequency and amplitude dependent effects. In general, increasing either stimulation frequency or amplitude decreases CE operating length-driving it towards the ascending limb; but has little effect on CE operating velocity (Fig. 7). When stimulation amplitude is held constant and frequency is varied, average operating length decreases as frequency increases (Fig. 7A). In general, lower frequencies have a greater *range* of CE operating velocities, but *average* CE operating velocity appears to be nearly uniform across frequency at 100% stimulation for cases where little to no passive force is required (i.e. $\omega_{stim} \geq 2.2$ Hz) (Fig. 7B).

When frequency is held constant at 2.8 Hz (or any frequency >1.6 Hz), increasing activation simultaneously decreases CE operating length and increases total excursion (Fig. 7C). Stimulation amplitude does not affect *average* operating velocity, but does influence the *range* of shortening velocities (Fig. 7D).

3.7. Mechanical power production

Greatest average positive MTU power output was observed in the 1.8–2.0 Hz range for stimulation amplitudes ranging from 60% to 100%; and in the 2.2–2.4 Hz range at 100% of maximum stimulation amplitude (Fig. 8A). CE average positive power was minimized when operating at frequencies greater than ~2.8 Hz (Fig. 8B). SEE average positive power was maximized in the range of 2.2–2.4 Hz for high amplitude stimulations ($\geq 80\%$) (Fig. 8C). For frequencies >1.6 Hz, the SEE contributed the majority of power, ranging anywhere from ~55–85% of total power production at stimulation amplitudes greater than 50% of maximum (Fig. 9). In general, increasing stimulation amplitude served to

increase contribution of SEE to total MTU positive power for all frequencies >2.0 Hz (Fig. 9).

3.8. Metabolic rate, MTU and CE apparent efficiency

In the range of stimulation frequency/amplitude which poses little to no risk of injury, average metabolic rate was highly dependent on stimulation amplitude (Fig. 10A). This is indicated by nearly horizontal contours of metabolic rate in 2.0–3.8 Hz range (Fig. 10A).

MTU apparent efficiency reached a maximal value of ~2.0 at 2.2 Hz (i.e. CE work/SEE work fraction=12.5%/87.5%, respectively, Fig. 9B), and declined with frequency to lows ~1.25 for the 3.6 Hz, 100% stim condition (i.e. CE work/SEE work fraction=20%/80%, respectively, Fig. 9B). MTU apparent efficiency was frequency dependent in regions that safely achieve hopping, as indicated by vertical contours (Fig. 10B).

CE apparent efficiency was strongly dependent on both frequency and amplitude of stimulation as indicated by the angled contours in Fig. 10C that safely achieve flight. CE apparent efficiency ranged from a low of ~0.2 at 4.0 Hz and 100% stimulation to a high of ~0.55 at 2.6 Hz and 50% stimulation.

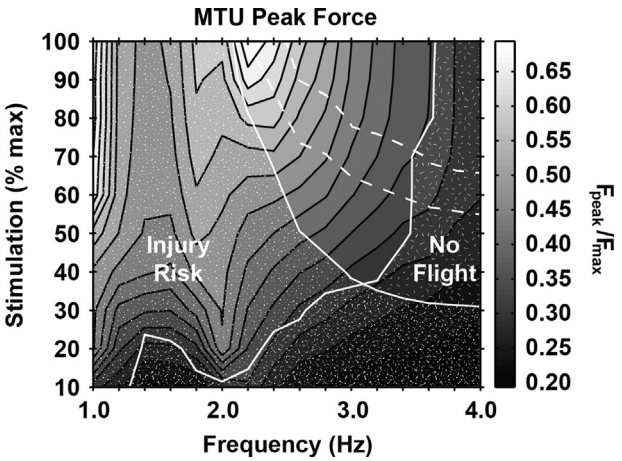

Fig. 4. Normalized peak MTU force (F_{peak}/F_{max}) (contours) versus stimulation frequency (x-axis) and amplitude (y-axis). Peak forces observed that achieve flight without posing injury risk were at 2.2 Hz and maximal (100%) stimulation. Dropping stimulation amplitude or raising/lowering frequency from this point resulted in reduced peak forces.

4. Discussion/conclusions

4.1. Stimulation frequency sets overall MTU mechanics

We expected that the neural stimulation strategy "tuned" to drive the human triceps-surae MTU at its passive resonant frequency ($\omega_{MTU\ resonance}=2.1$ Hz) would maximize MTU force and SEE elastic energy storage and at the same time minimize CE length changes and mechanical power output (i.e. optimal "tuning"). In contrast to our expectation, the frequency at which maximal MTU force and SEE energy cycling occurred was 2.2 Hz, slightly higher than the predicted value of 2.1 Hz from hypothesis (1) (Fig. 4).

Our hypothesis that optimal tuning would occur at 2.1 Hz was based on the fundamental principle from linear systems theory

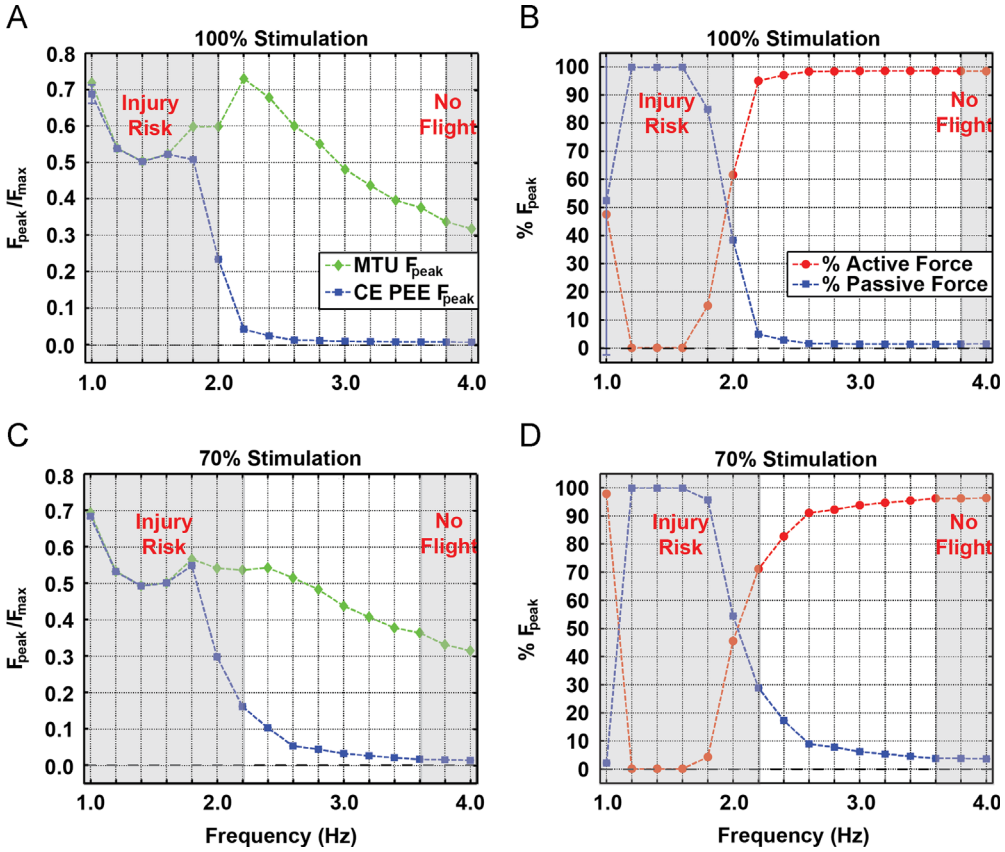

Fig. 5. Contour slice of MTU and passive CE peak force, as well as their % contribution to total force, for stimulation amplitudes of 100% (A and B, respectively) and 70% (C and D, respectively). Conditions that pose excessive risk of injury or do not achieve a flight phase are indicated by opaque gray regions. Note that both higher frequencies and amplitudes of stimulation have less dependence on passive CE force generation.

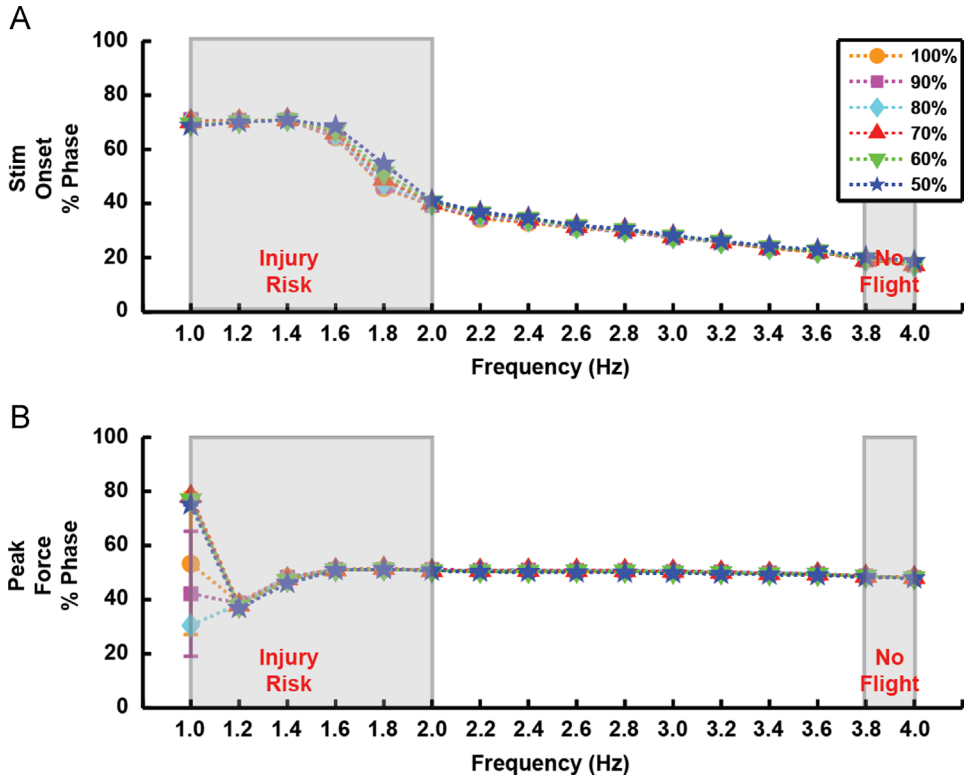

Fig. 6. Phasing of stimulation onset (A) and peak force (B) relative to minimum MTU length at all frequencies of stimulation for amplitudes ranging from 50% to 100% of maximum. Conditions with elevated injury risk and no flight phase for the 100% stimulation amplitude condition are indicated by opaque gray regions. Note that, for frequencies > 1.4 Hz, stimulation onset occurs earlier relative to minimum MTU length as frequency is increased, while peak force phasing remains constant.

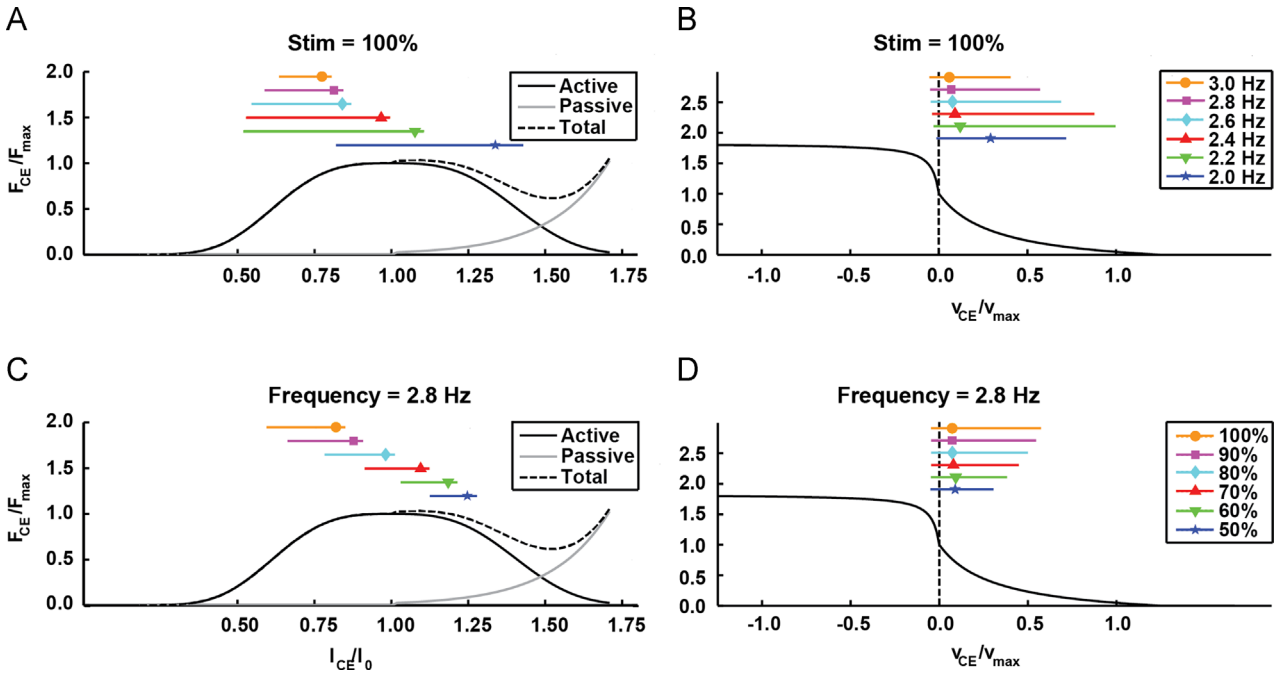

Fig. 7. Normalized CE force–length (F–L) and –velocity (F–V) operating point for a range of frequencies at maximum stimulation amplitude (A and B, respectively) and a range of stimulation amplitudes at 2.8 Hz (C and D, respectively). The range of F–L and F–V operating conditions during active force production is indicated by color-coded bars, and the average operating point is indicated by a marker placed over each bar. Note that both frequency and magnitude of stimulation modulate force–length operating point (A and C), while there is little effect of either parameter on average operating velocity for frequencies > 2.0 Hz (B and D). (For interpretation of the references to color in this figure legend, the reader is referred to the web version of this article.)

that driving a spring–mass system at its natural frequency would lead to resonant behavior (Ogata, 2003). Lack of optimal "tuning" at 2.1 Hz was due, in large part, to the fact that MTU stiffness was determined by the *both* passive and active tissues (i.e. CE). For example, when considering only passive components (k_{CE} and k_{SEE}) of the spring–mass system the resonant frequency is $\sim$2.1 Hz ($k_{MTU} \sim 60{,}000\, N/m$). On the other hand, during an isometric contraction when the active component of the CE stiffens and

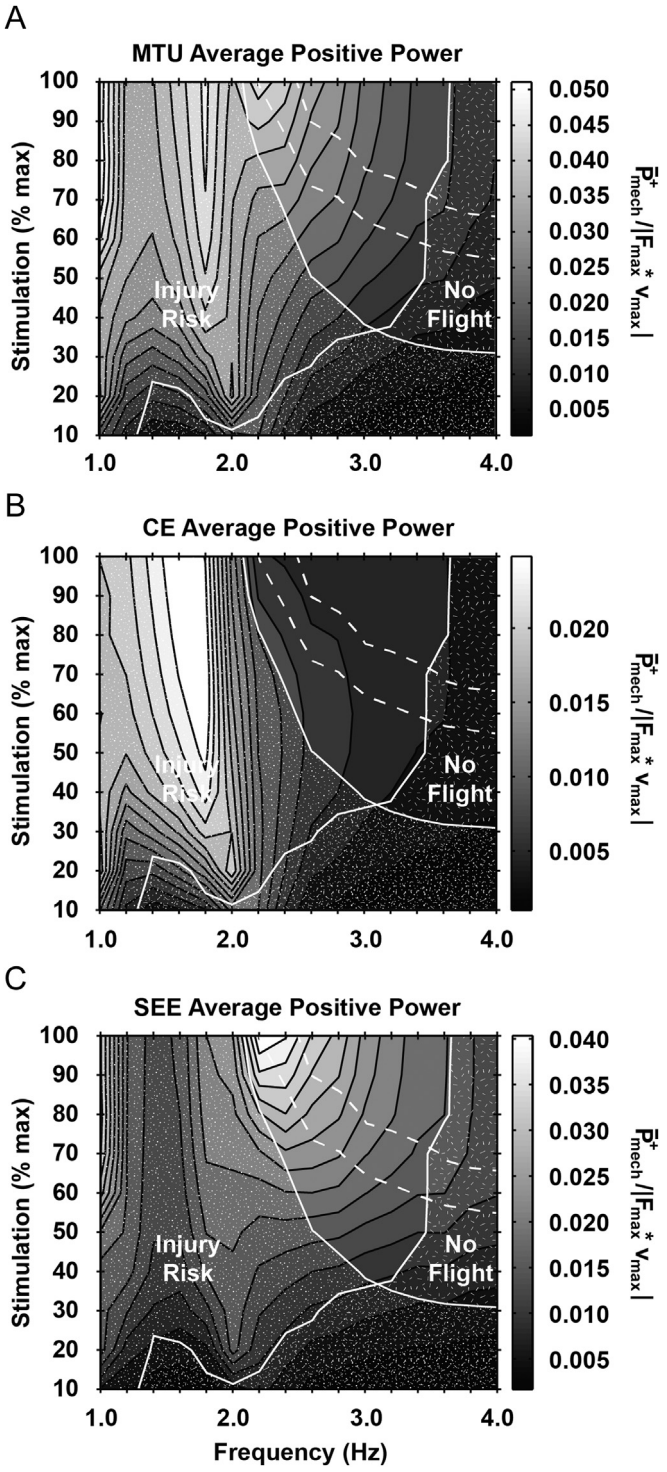

Fig. 8. Average positive power produced in the MTU (A), CE (B), and SEE (C) (contours) for all stimulation frequency (x-axis) and amplitude (y-axis) combinations. All values are normalized to $|F_{max} \times v_{max}|$ (Table 1). Note that MTU average positive power generally trends with frequency (i.e. nearly vertical contours) (A), CE positive power is relatively constant (B), and SEE power is has both frequency and amplitude dependence (i.e. diagonal contours) (C) in regions where hopping is safely achieved.

become strut-like, the SEE is left as the only "spring-like" component of the MTU. In this case the resonant frequency would be $\sim$3.8 Hz ($k_{MTU} = k_{SEE} \approx 120,000\ N/m$). Essentially, shifts in the non-linear F–L and F–V dynamics of the CE determined by its active state dynamically change its impedance (Farahat and Herr, 2010). This makes it very difficult to predict the frequency response of muscle-driven systems a priori based on system parameters.

4.2. Frequency and phasing: the role of CE operating length

CE length at which stimulation onset occurred was critical in determining both the safety and functional efficacy of MTU mechanics. For nearly all frequencies explored here ($\omega_{stim} > 1.4$ Hz), peak MTU force occurred almost exactly 50% of a stimulation cycle after the MTU reached its minimum length. This phenomena was entirely frequency dependent, and not influenced by changes in stimulation amplitude (Fig. 6B). In the case of frequencies from 1.6 to 1.8 Hz this phasing was purely the result of passive mechanics, as demonstrated by peak forces *preceding* stimulation onset (Figs. 5 and 6). Under these conditions, muscle was stretched to injurious strains, and activated against a shortening SEE (Fig. 3B). This not only results in high CE positive power production (Fig. 8B) and metabolic rates due to rapid CE shortening (Fig. 10A), but also relatively low SEE positive power production (Fig. 8C) and MTU efficiency (Fig. 10B).

This trend starts to reverse with the 2.0 Hz condition. While there is still high risk of injury due to loading of the MTU prior to stimulation onset (Figs. 2A and 3B), it does occur prior to observed peak forces (Fig. 6). As stimulation frequency is increased, stimulation onset occurs earlier relative to minimum MTU length (Fig. 6) and at lower CE strains resulting in reduced injury risk (Figs. 2 and 3B). Stimulation frequencies $>$2.0 Hz also facilitate muscle activation on/near the crest of the CE F–L curve during lengthening, resulting in high total/active CE force production (Figs. 4 and 5), low positive power output in the CE (Fig. 8B), high positive power production from the MTU/SEE (Fig. 8A and C), reduced metabolic rate (Fig. 10A) and increased MTU efficiency (Fig. 10B). These ideal mechanics/energetics are observed for an operational bandwidth of $\sim$2.2–3.4 Hz. Above this frequency, the CE is not allowed adequate time to lengthen, and active force production occurs exclusively on the ascending portion of the F–L curve (Fig. 7A). This results in lower peak forces (Fig. 4), and an inability to meet task demands for hopping (Fig. 3A).

In contradiction with hypothesis (2), however, minimal CE work/average positive power output did not occur at $\omega_{MTU\ resonance} =$ 2.1 Hz. Rather, minimal/low CE work was observed for stimulation frequencies $>$2.4 Hz (Fig. 8B). Stimulation onset timing in these conditions is such that there is no undue stretch and recoil (i.e. mechanical work) performed by the CE PEE. While stimulation amplitude also plays a role in this phenomena (discussed below), frequency played a critical role in regulating CE operating length at stimulation onset, and was solely responsible for phasing of stimulation onset and peak force (Fig. 6).

4.3. Stimulation amplitude adjusts within MTU mechanics

In agreement with hypothesis (3), stimulation amplitude controlled MTU force as well as relative contributions of CE versus SEE to overall power output of the MTU. Stimulation amplitude, in conjunction with frequency, can also modulate operating length of the CE (Fig. 7C) and therefore active/passive force sharing (Figs. 3B and 5). In general, higher stimulation amplitude leads to shorter CE operating lengths and thus low or no CE passive force (Figs. 3B, 5, and 7C). This effect was most pronounced where lack of adequate stimulation forced the CE to shift from ascending portions to the crest of F–L, and even onto the descending limb where the CE PEE could compensate for reduced active CE force production (Figs. 3B and 7C).

Muscle stimulation amplitude was an effective means of modulating injury risk and the portion of MTU power output that came from elastic energy storage and return versus active muscle shortening. While stimulation amplitude did not significantly affect

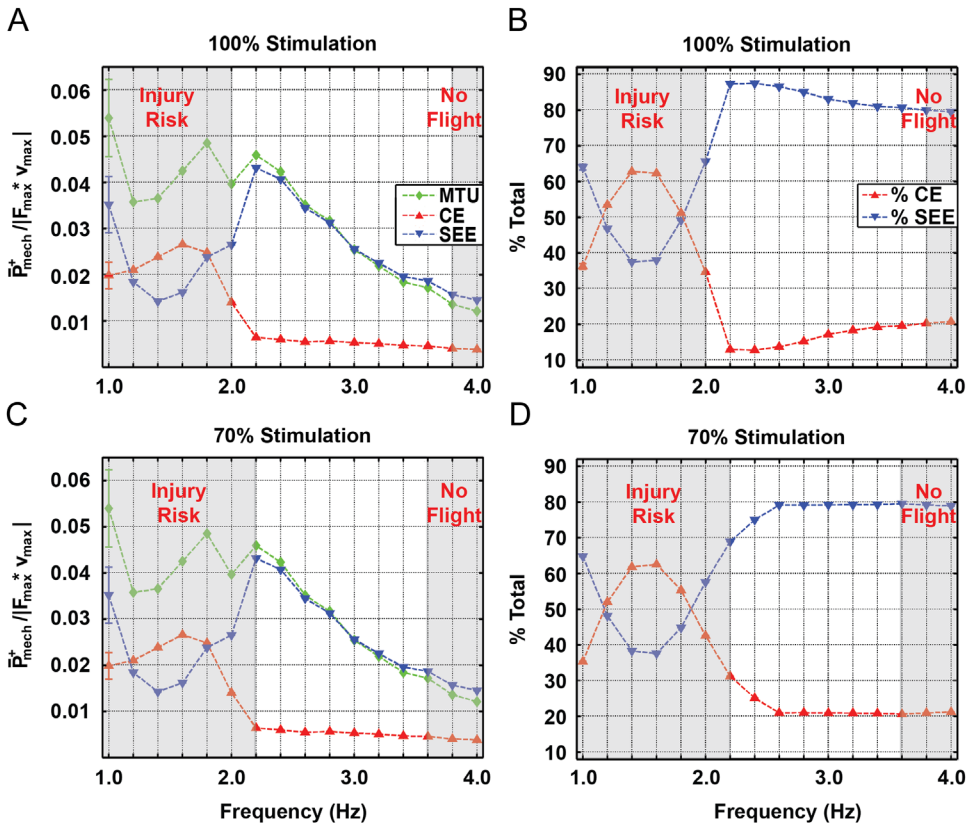

Fig. 9. Normalized average positive power produced by MTU, CE, and SEE, as well as % contributions from CE and SEE at all stimulation frequencies for amplitudes of 100% (A and B, respectively) and 70% (C and D, respectively). Regions of high injury risk and no flight are indicated by opaque gray areas. Note that the majority of positive power comes from the SEE for stimulation frequencies >1.8 Hz for both stimulation amplitudes.

CE positive power, as indicated by nearly vertical (i.e. frequency dependent) contours (Fig. 8B); it did have an impact on both MTU and SEE average positive power as indicated by diagonal (i.e. stimulation frequency and amplitude dependent) contours (Fig. 8A and C). The most notable effect of stimulation amplitude on power output was how it was *shared* between CE and SEE. For example, at a stimulation frequency of 2.2 Hz with an amplitude of 70%, there is high injury risk and 30–70% power sharing in CE and SEE, respectively (Fig. 9D). By increasing stimulation amplitude to 100%, risk of injury can be eliminated and CE-SEE power sharing is 10–90% (Fig. 9B).

4.4. Role of stimulation frequency and amplitude on metabolic rate and efficiency

Our hypothesis that (4) metabolic rate and MTU apparent efficiency are maximized at the passive resonant frequency (2.1 Hz) was not supported in its entirety. Metabolic rate was almost entirely dependent on stimulation amplitude, as indicated by horizontal contours in Fig. 10A. This is somewhat unexpected given that our metabolic cost model also possessed a strong velocity dependence; but is consistent with the observation that varying frequency in the range of 2.2–3.0 Hz does very little to influence the average operating velocity of the CE during active force production (Fig. 7B).

By modulating stimulation frequency in a compliant MTU, it is possible to achieve a constant metabolic "rate of return" (e.g. MTU apparent efficiency) regardless of amplitude (Fig. 10B). Stimulation amplitude primarily governed power sharing between CE and SEE (Figs. 5 and 9). Its role was to regulate the trade-off between high force production with significant SEE energy storage and return (Figs. 4 and 8C), or force compensation via CE PEE recoil resulting in lower metabolic demand (Fig. 10A), greater CE efficiency (Fig. 10C), and increased risk of injury (Fig. 3B). The combination of these factors resulted in peak MTU apparent efficiency at a stimulation frequency of 2.2 Hz (Fig. 10B), and peak CE apparent efficiency occurring for stimulation amplitudes that operate with strains on the cusp of injury at all frequencies between 2.2 and 3.2 Hz (Figs. 3B and 10C). Above this frequency band increased stimulation amplitude is required to achieve a flight phase, resulting in reduced muscle strains/CE PEE utilization (Fig. 3B), increased metabolic rate (Fig. 10A), and ultimately reduced CE apparent efficiency (Fig. 10C).

4.5. Minimizing metabolic cost while avoiding muscle injury—a trade-off criterion that drives movement preference?

Trying to determine what, if any, mechanical and energetic criteria humans seek to optimize in bouncing gait is a daunting task. Lower frequencies of movement (i.e. 2.2–2.4 Hz) require high mechanical power output (Fig. 8A) and stimulation amplitude/metabolic rate (Fig. 10A), but also most effectively utilize series elastic tissues (Fig. 8C) and have the greatest apparent efficiency of movement (Fig. 10B). Intermediate frequencies of movement (i.e. 2.6–3.0 Hz) require the lowest stimulation amplitudes to safely hop (Fig. 3B) reducing overall metabolic demand (Fig. 10A) and increasing CE apparent efficiency (Fig. 10C). These benefits, however, come at the cost of increased CE PEE strains and injury risk (Fig. 3B), reduced contributions from the SEE (Fig. 8C), and decreased MTU apparent efficiency (Fig. 10B). High frequencies of movement (e.g. >3.2 Hz) force the CE onto its ascending limb (Fig. 3B), reducing its capacity to actively produce force. These high frequencies of movement also necessitate greater rates of force to achieve hopping, ultimately requiring higher stimulation amplitudes and increased metabolic rates (Figs. 3A and 10A).

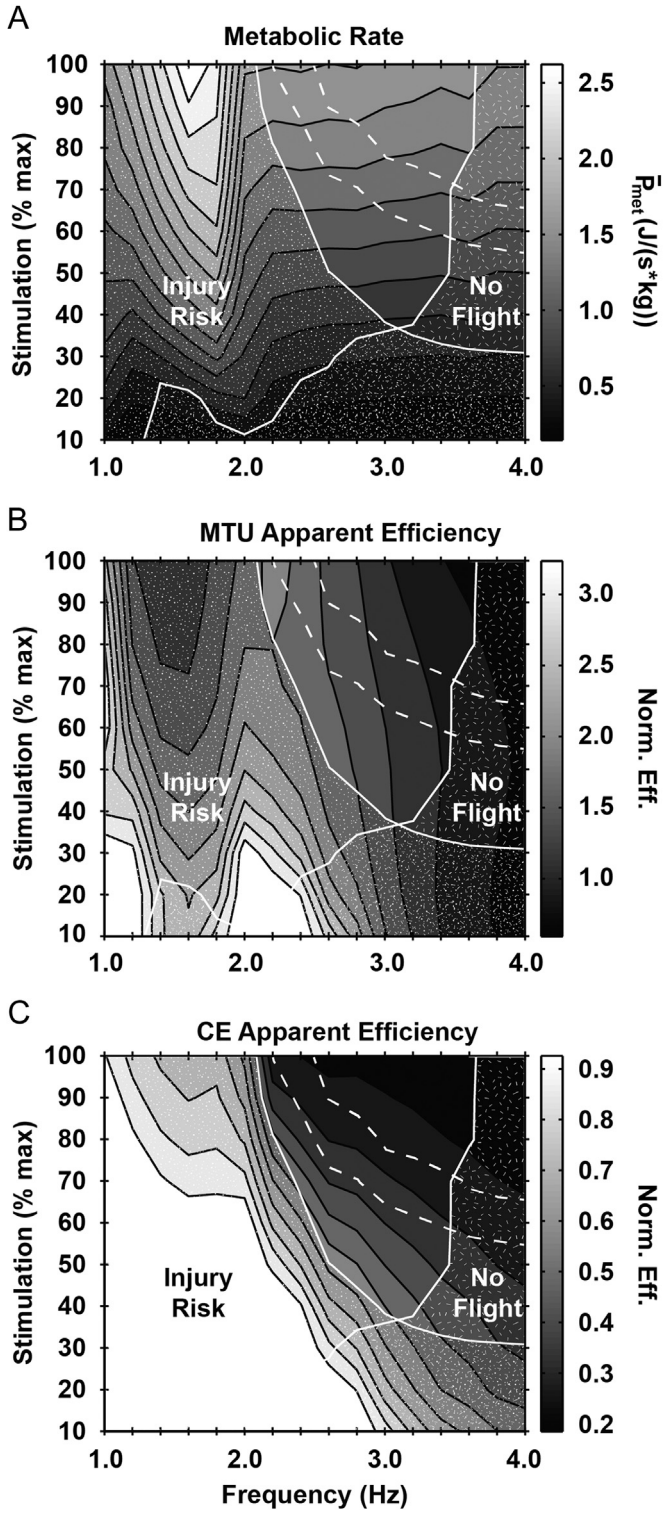

Fig. 10. Average metabolic rate (J/(s kg)) (A), and apparent efficiency (P^{+}_{mech}/P_{met}) of the MTU (B) and CE (C) (contours) versus stimulation frequency (*x*-axis) and amplitude (*y*-axis). Conditions with high risk of injury (speckled) or no flight (hatched) are filled and bordered in white. Note that metabolic rate was entirely stimulation amplitude dependent (i.e. horizontal contours) (A), MTU apparent efficiency was entirely frequency dependent (i.e. vertical contours) (B), and CE apparent efficiency is dependent on both (i.e. diagonal contours) (C) in regions where hopping is safely achieved.

While there are conflicting trends in metabolic cost for human hopping, the spectrum of experimental outcomes can be observed in our modeled data depending on how parameter space is traversed. Based on Farris et. al., one would expect increases in metabolic cost beyond operating frequencies of ~2.8 Hz (Farris and Sawicki, 2012). Based on trends from Gutmann (2011) and Grabowski and Herr (2009), however, it would be expected that metabolic rate would continue to decline as stimulation frequency is increased. In our modeled data, the range of stimulation frequency/amplitude combinations that facilitate hopping are limited by injury risk and the ability to achieve an aerial phase. Using 2.2 Hz and 100% stimulation amplitude as a starting point, our model predicts that it is possible to safely and effectively trade lower stimulation amplitude for increasing stimulation frequency until ~2.8–3.2 Hz (Fig. 3). This would result in reduced metabolic rate, a direct correlate with stimulation amplitude (Fig. 10A). It can also be seen that, as frequency is increased, it becomes necessary to also increase stimulation amplitude to achieve an aerial phase for stimulation frequencies >3.2 Hz (the highest frequency condition from Farris and Sawicki (2012) and Gutmann (2011) (Fig. 3A). It is not possible to predict human preference based on our model, but if people employ a strategy to minimize activation while avoiding injury risk during frequency constrained hopping, experimentally observed trends in metabolic rate mesh well with those predicted here.

4.6. Future directions

Despite its inherent simplicity, the model presented here provides ample insight into the role of neural control in shaping compliant MTU mechanics and energetics. Emergent behaviors from this model that correspond remarkably well to observed human mechanics include ground reaction force (i.e. MTU force) profiles (Farris and Sawicki, 2012; Farley et al., 1991; Ferris et al., 2006; Gutmann, 2011; Grabowski and Herr, 2009; Chang et al., 2008), near isometry in the CE (Farris et al., 2013), effective SEE energy cycling (Farris et al., 2013), and frequency dependent minimums in metabolic cost (Farris and Sawicki, 2012; Gutmann, 2011; Grabowski and Herr, 2009). This baseline model is meant to serve as the backbone for an in silico testbed to optimize assistive exoskeleton technologies designed to improve human performance in bouncing gaits. Thus, in future research we will extend the current model to (1) explore the influence that parallel assistive devices (e.g. elastic exoskeletons) have on compliant MTU mechanics and energetics during steady cyclic movements and (2) assess the interplay between MTU morphology and afferent feedback pathways during perturbed movements with and without assistive devices.

References

Alexander, R.M., 2002. Tendon elasticity and muscle function. Comp. Biochem. Physiol. A: Mol. Integr. Physiol. 133, 1001–1011 (Dec).
Alexander, R.M., 1997. Optimum muscle design for oscillatory movements. J. Theor. Biol. 184, 253–259.
Arnold, E.M., Delp, S.L., 2011. Fibre operating lengths of human lower limb muscles during walking. Philos. Trans. R. Soc. Lond. B: Biol. Sci. 366 (May), 1530–1539.
Arnold, E.M., Hamner, S.R., Seth, A., Millard, M., Delp, S.L., 2013. How muscle fiber lengths and velocities affect muscle force generation as humans walk and run at different speeds. J. Exp. Biol. 216 (June), 2150–2160.
Ackermann, M., van den Bogert, A.J., 2010. Optimality principles for model-based prediction of human gait. J. Biomech. 43 (April), 1055–1060.
Azizi, E., Brainerd, E.L., Roberts, T.J., 2008. Variable gearing in pennate muscles. Proc. Natl. Acad. Sci. U.S.A. 105 (February), 1745–1750.
Azizi, E., Roberts, T.J., 2010. Muscle performance during frog jumping: influence of elasticity on muscle operating lengths. Proc. Biol. Sci. 277 (May), 1523–1530.
Blickhan, R., 1989. The spring-mass model for running and hopping. J. Biomech. 22, 1217–1227.
Bobbert, M.F., Huijing, P.A., van Ingen Schenau, G.J., 1986. A model of the human triceps surae muscle–tendon complex applied to jumping. J. Biomech. 19, 887–898.
Biewener, A.A., Farley, C.T., Roberts, T.J., Temaner, M., 2004. Muscle mechanical advantage of human walking and running: implications for energy cost. J. Appl. Physiol. 97 (December), 2266–2274.

Brooks, S.V., Zerba, E., Faulkner, J.A., 1995. Injury to muscle fibres after single stretches of passive and maximally stimulated muscles in mice. J. Physiol. 488 (October (Pt 2)), 459–469.
Carrier, D.R., Anders, C., Schilling, N., 2011. The musculoskeletal system of humans is not tuned to maximize the economy of locomotion. Proc. Natl. Acad. Sci. U.S.A. 108 (November), 18631–18636.
Carrier, D.R., Heglund, N.C., Earls, K.D., 1994. Variable gearing during locomotion in the human musculoskeletal system. Science 265 (July), 651–653.
Chang, Y.H., Roiz, R.A., Auyang, A.G., 2008. Intralimb compensation strategy depends on the nature of joint perturbation in human hopping. J. Biomech. 41, 1832–1839.
Dean, J.C., Kuo, A.D., 2011. Energetic costs of producing muscle work and force in a cyclical human bouncing task. J. Appl. Physiol. 110 (April), 873–880.
Doke, J., Kuo, A.D., 2007. Energetic cost of producing cyclic muscle force, rather than work, to swing the human leg. J. Exp. Biol. 210 (July), 2390–2398.
Farley, C.T., Morgenroth, D.C., 1999. Leg stiffness primarily depends on ankle stiffness during human hopping. J. Biomech. 32 (March), 267–273.
Farris, D.J., Sawicki, G.S., 2012. Linking the mechanics and energetics of hopping with elastic ankle exoskeletons. J. Appl. Physiol. 113 (December), 1862–1872.
Farley, C.T., Blickhan, R., Saito, J., Taylor, C.R., 1991. Hopping frequency in humans: a test of how springs set stride frequency in bouncing gaits. J. Appl. Physiol. 71 (December), 2127–2132.
Fung, Y.C., 1967. Elasticity of soft tissues in simple elongation. Am. J. Physiol. 213 (December), 1532–1544.
Farris, D.J., Robertson, B.D., Sawicki, G.S., 2013. Passive elastic exoskeletons reduce soleus muscle force but not work in human hopping. J. Appl. Phys. 115 (September), 579–585.
Ferris, D.P., Bohra, Z.A., Lukos, J.R., Kinnaird, C.R., 2006. Neuromechanical adaptation to hopping with an elastic ankle-foot orthosis. J. Appl. Physiol. 100 (January), 163–170.
Fukunaga, T., Roy, R.R., Shellock, F.G., Hodgson, J.A., Day, M.K., Lee, P.L., et al., 1992. Physiological cross-sectional area of human leg muscles based on magnetic resonance imaging. J. Orthop. Res. 10 (November), 928–934.
Farahat, W.A., Herr, H.M., 2010. Optimal workloop energetics of muscle-actuated systems: an impedance matching view. PLoS Comput. Biol. 6 (June), e1000795.
Geyer, H., Seyfarth, A., Blickhan, R., 2006. Compliant leg behaviour explains basic dynamics of walking and running. Proc. Biol. Sci. 273 (November), 2861–2867.
Gutmann, A.K., 2011. Human Hopping: A Model for Understanding the Mechanics and Energetics of Bouncing Gaits (Ph.D.). Department of Medical Science, University of Calgary, Calgary.
Grabowski, A.M., Herr, H.M., 2009. Leg exoskeleton reduces the metabolic cost of human hopping. J. Appl. Physiol. 107 (September), 670–678.
Hof, A.L., Van Zandwijk, J.P., Bobbert, M.F., 2002. Mechanics of human triceps surae muscle in walking, running and jumping. Acta Physiol. Scand. 174 (January), 17–30.
Holt, K.G., Hamill, J., Andres, R.O., 1990. The force-driven harmonic-oscillator as a model for human locomotion. Hum. Movement Sci. 9 (February), 55–68.
Haeufle, D.F., Grimmer, S., Seyfarth, A., 2010. The role of intrinsic muscle properties for stable hopping—stability is achieved by the force–velocity relation. Bioinspir. Biomim. 5 (March), 16004.
Haeufle, D.F., Grimmer, S., Kalveram, K.T., Seyfarth, A., 2012. Integration of intrinsic muscle properties, feed-forward and feedback signals for generating and stabilizing hopping. J. R. Soc. Interface January.
Hill, A.V., 1938. The heat of shortening and the dynamic constants of muscle. Proc. R. Soc. Lond. Ser. B: Biol. Sci. 126 (October), 136–195.
Ishikawa, M., Komi, P.V., Grey, M.J., Lepola, V., Bruggemann, G.P., 2005. Muscle–tendon interaction and elastic energy usage in human walking. J. Appl. Physiol. 99 (August), 603–608.
Krishnaswamy, P., Brown, E.N., Herr, H.M., 2011. Human leg model predicts ankle muscle–tendon morphology, state, roles and energetics in walking. PLoS Comput. Biol. 7 (March), e1001107.
Kuo A.D., Donelan J.M., Ruina A. Energetic consequences of walking like an inverted pendulum: step-to-step transitions. Exerc Sport Sci Rev. 2005 Apr;33(2):88–97.
Lichtwark, G.A., Bougoulias, K., Wilson, A.M., 2007. Muscle fascicle and series elastic element length changes along the length of the human gastrocnemius during walking and running. J. Biomech. 40, 157–164.
Lichtwark, G.A., Wilson, A.M., 2008. Optimal muscle fascicle length and tendon stiffness for maximising gastrocnemius efficiency during human walking and running. J. Theor. Biol. 252 (June), 662–673.
Lichtwark, G.A., Wilson, A.M., 2007. Is Achilles tendon compliance optimised for maximum muscle efficiency during locomotion? J. Biomech. 40, 1768–1775.
Lieber, R.L., Friden, J., 1993. Muscle damage is not a function of muscle force but active muscle strain. J. Appl. Physiol. 74 (February), 520–526.
Lieber, R.L., Leonard, M.E., Brown, C.G., Trestik, C.L., 1991a. Frog semitendinosis tendon load-strain and stress-strain properties during passive loading. Am. J. Physiol. 261 (July), C86–C92.
Lieber, R.L., Woodburn, T.M., Friden, J., 1991b. Muscle damage induced by eccentric contractions of 25% strain. J. Appl. Physiol. 70 (June), 2498–2507.
Monsch, E.D., Franz, C.O., Dean, J.C., 2012. The effects of gait strategy on metabolic rate and indicators of stability during downhill walking. J. Biomech. 45 (July), 1928–1933.
Minetti, A.E., Alexander, R.M., 1997. A theory of metabolic costs for bipedal gaits. J. Theor. Biol. 186 (June), 467–476.
Maykranz, D., Grimmer, S., Seyfarth, A., 2013. A work-loop method for characterizing leg function during sagittal plane movements. J. Appl. Biomech. 29 (October), 616–621.
Morgan, D.L., Allen, D.G., 1999. Early events in stretch-induced muscle damage. J. Appl. Physiol. 87 (December), 2007–2015.
Ma, S.P., Zahalak, G.I., 1991. A distribution-moment model of energetics in skeletal muscle. J. Biomech. 24, 21–35.
Neptune, R.R., McGowan, C.P., 2011. Muscle contributions to whole-body sagittal plane angular momentum during walking. J. Biomech. 44 (January), 6–12.
Neptune, R.R., McGowan, C.P., Kautz, S.A., 2009. Forward dynamics simulations provide insight into muscle mechanical work during human locomotion. Exerc. Sport Sci. Rev. 37 (October), 203–210.
Otten, E., 1987. A myocybernetic model of the jaw system of the rat. J. Neurosci. Methods 21 (October), 287–302.
Ogata, K., 2003. System Dynamics, 4th ed. Prentice Hall, Upper Saddle River, NJ
Roberts, T.J., 2002. The integrated function of muscles and tendons during locomotion. Comp. Biochem. Physiol. A: Mol. Integr. Physiol. 133 (December), 1087–1099.
Raburn, C.E., Merritt, K.J., Dean, J.C., 2011. Preferred movement patterns during a simple bouncing task. J. Exp. Biol. 214 (November), 3768–3774.
Rubenson, J., Pires, N.J., Loi, H.O., Pinniger, G.J., Shannon, D.G., 2012. On the ascent: the soleus operating length is conserved to the ascending limb of the force–length curve across gait mechanics in humans. J. Exp. Biol. July.
Raasch, C.C., Zajac, F.E., Ma, B., Levine, W.S., 1997. Muscle coordination of maximum-speed pedaling. J. Biomech. 30 (June), 595–602.
Srinivasan, M., Holmes, P., 2008. How well can spring-mass-like telescoping leg models fit multi-pedal sagittal-plane locomotion data? J. Theor. Biol. 255 (November), 1–7.
Srinivasan, M., 2011. Fifteen observations on the structure of energy-minimizing gaits in many simple biped models. J. R. Soc. Interface 8 (January), 74–98.
Snyder, K.L., Farley, C.T., 2011. Energetically optimal stride frequency in running: the effects of incline and decline. J. Exp. Biol. 214 (June), 2089–2095.
Sawicki, G.S., Ferris, D.P., 2008. Mechanics and energetics of level walking with powered ankle exoskeletons. J. Exp. Biol. 211 (May), 1402–1413.
Takeshita, D., Shibayama, A., Muraoka, T., Muramatsu, T., Nagano, A., Fukunaga, T., et al., 2006. Resonance in the human medial gastrocnemius muscle during cyclic ankle bending exercise. J. Appl. Physiol. 101 (July), 111–118.
Umberger, B.R., Rubenson, J., 2011. Understanding muscle energetics in locomotion: new modeling and experimental approaches. Exerc. Sport Sci. Rev. 39 (April), 59–67.
Umberger, B.R., Gerritsen, K.G., Martin, P.E., 2003. A model of human muscle energy expenditure. Comput. Methods Biomech. Biomed. Eng. 6 (April), 99–111.
van der Krogt, M.M., de Graaf, W.W., Farley, C.T., Moritz, C.T., Richard Casius, L.J., Bobbert, M.F., 2009. Robust passive dynamics of the musculoskeletal system compensate for unexpected surface changes during human hopping. J. Appl. Physiol. 107 (September), 801–808.
Winters, J.M., Stark, L., 1988. Estimated mechanical properties of synergistic muscles involved in movements of a variety of human joints. J. Biomech. 21, 1027–1041.
Zajac, F.E., 1989. Muscle and tendon: properties, models, scaling, and application to biomechanics and motor control. Crit. Rev. Biomed. Eng. 17, 359–411.